Journal of Molecular Liquids 421 (2025) 126922

Contents lists available at ScienceDirect

Journal of Molecular Liquids

journal homepage: www.elsevier.com/locate/molliq

Intramolecular H-bond properties in Solvated Cyclodextrins Elucidated by SAXS and molecular Dynamics simulation☆

Imre Bakó [a], András Wacha [a], Szilvia Pothoczki [b,*]

[a] HUN-REN Research Centre for Natural Sciences H-1117 Budapest, Magyar tudósok körútja 2, Hungary
[b] HUN-REN Wigner Research Centre for Physics H-1121 Budapest, Konkoly-Thege M. út 29-33, Hungary

ARTICLE INFO

Keywords:
Molecular Dynamics simulation
SAXS
H-bond properties

ABSTRACT

The structural rigidity of cyclodextrin (CD) molecules, which plays a leading role in their ability to form inclusion complexes, is largely due to the hydrogen bonds (HBs) formed within the CD molecule. To describe these intramolecular HB properties we performed Molecular Dynamics (MD) simulations for α-, β-, and γ-CD molecules in an aqueous environment. We scrutinized the role of tumbling phenomenon, that is, the glucopyranose (Glc*p*) units may rotate around the glycosidic bonds, in formation of intramolecular HBs. As a first step the tumbling of Glc*p* units were characterized and different water model were applied to monitor their effects on the ratio of rotated cases. The results show that this ratio can highly depend on the applied water model. Small-angle X-ray diffraction experiments were performed. A comparison of the molecular shape factors obtained from MD simulations and SAXS experiments reveals a low probability of tumbling of Glc*p* units. This result corresponds with the calculated average probability of rotated Glc*p* unit from MD simulation for α-CD and β-CD. However, it significantly deviates in the case of γ-CD.

1. Introduction

Cyclodextrins (CDs) have received considerable attention for their unique structural properties and ability to form inclusion complexes with many guest molecules. [1–3] Detailed summaries of the scientific and technological aspects of CDs, including their synthesis, reactivity, as well as chemical, biological, and medical applications are available in several review studies (e.g. [4–6]). The three most prevalent CDs are α-cyclodextrin (α-CD), β-cyclodextrin (β-CD), and γ-cyclodextrin (γ-CD), which are composed of six, seven, and eight 1,4-linked D-glucopyranoside (Glc*p*) units, respectively. The presence of three hydroxyl groups within the Glc*p* units can participate in hydrogen bonds (H-bonds) formation in aqueous solutions, playing a crucial role in various intermolecular interactions. The secondary hydroxyl groups form a strongly hydrophilic barrier over the significantly less hydrophilic cavity. Besides these intermolecular interactions, the structural rigidity of CD molecules provided by intramolecular H-bonding is a determining factor in the complex host–guest processes in these systems. [7–10] An understanding of the characteristics of these hydrogen bond connections within the CD molecule is essential for detailed comprehension of these processes.

Experimental results showed that in the crystalline α-CD-hexahydrate, at least one Glc*p* unit may rotate around the glycosidic bonds. [10–12] This process is often called tumbling of the Glc*p* unit(s). [13] In addition, it has been shown that this flexibility can facilitate the formation of the guest–host complex for other CD complexes. [14,15] Unfortunately, no direct experimental information exists on how often these sugar unit rotations occur around the glycosidic bonds in aqueous solutions containing only native CDs. [13] However, NMR spectroscopy has already detected CD dimers linked by different types of molecules. [16–18] Molecular dynamics simulations have revealed that the tumbling of Glcp units in aqueous solutions is particularly common in γ-CD. Additionally, the specific force field model used for the CD molecules significantly influences the frequency of this tumbling, as the studies demonstrated. [13,19] However, the investigation into the potential impact of the applied water model on the tumbling process or the effect of this tumbling on the intramolecular H-bonds received less attention.

Our main goal was to study how various water models influence the probability of Glc*p* units tumbling and the effects of this tumbling on intramolecular hydrogen bonding properties. It is necessary to point out that intramolecular H-bonding detection in CDs is challenging. [20] The

☆ This article is part of a special issue entitled: 'Idrissi 60 Festschrift' published in Journal of Molecular Liquids.

* Corresponding author.
E-mail address: pothoczki.szilvia@wigner.hun-ren.hu (S. Pothoczki).

https://doi.org/10.1016/j.molliq.2025.126922
Received 8 November 2024; Received in revised form 8 January 2025; Accepted 9 January 2025
Available online 11 January 2025

formation of H-bonds between the two secondary hydroxyl groups of adjacent Glc*p* units at the wider rim of the CD molecule is not in question, it is commonly referred to as imparts the above-mentioned structural rigidity. [7–10] However, H-bonds between the two secondary hydroxyl groups within the same Glc*p* unit remain a subject of debate, because several quantum chemical descriptors (e.g. bond critical point) are unsuitable for this H-bond detection. [20,21]. The existence of an H-bond between the two neighboring primary hydroxyl groups at the narrower rim is also controversial. Primarily, quantum chemical studies indicate that in these most stable CD conformers, a well-defined H-bonding network is also formed between the primary hydroxide groups. [20,21] On the other hand, experimental results suggest that these hydroxyl groups are quite distant from each other and thus cannot form H-bonds. [22].

Therefore, extensive molecular dynamics simulations were performed for α-, β-, and γ-CDs in aqueous solution. We applied five commonly used water models [23–28] to examine their performance in respect of occurrences of tumbling. To elucidate this tumbling process we present its time evolution, the number, and the mutual position of rotated units. To the reveal effects of tumbling on structural properties, we calculated typical dihedrals and intra-molecular H-bond characteristics to the whole trajectory and separately those cases where rotated unit appeared or not.

To validate our calculations small-angle X-ray scattering (SAXS) provides a strong base and is appropriate to answer the above-mentioned questions. [29,30] Several studies utilizing SAXS experiments provided insights into the aggregation of CD in aqueous solutions. [31–35] In this study, we extend our analysis to a broader Q range to obtain information not only about the aggregation and molecule size but also about the conformation of glucopyranoside unit arrangements. Calculating molecular form factors can give us more detailed information about the tumbling process. To determine whether the rotated structure is significantly present in the solutions, we compare the calculated and the measured molecular form factors.

2. Materials and Methods

2.1. Materials

Chemicals, α-CD (≥98 %), β-CD (≥97 %), and γ-CD (≥98 %) powders, were purchased from Sigma-Aldrich and used without further purification. Aqueous solutions were prepared by dissolving these powders in deionized water. Two concentrations of each substance were prepared: a dilute solution and a solution near the solubility limit ("concentrated"). The CD: water molar ratios in aqueous solutions were 1:415.1 (11.51 wt%) and 1:827.9 (6.12 wt%) for α-CD; 1:3700.4 (1.67 wt%) and 1:7377.7 (0.85 wt%) for β-CD; 1:310.2 (18.84 wt%) and 1:612.2 (10.52 wt%) for γ-CD.

2.2. Small-angle X-ray scattering

Small-angle X-ray scattering measurements were performed using CREDO, an in-house transmission geometry set-up [36,37]. For the experiments, 1.2 mm outer thin-walled quartz capillaries were used. For the measurements, CuKα (0.1542 nm wavelength) monochromatized and collimated X-rays were employed in a variable scattering range of 0.23–10.2 nm^{-1}. A detailed description of data processing can be found in the following literature. [36,37].

2.3. Simulation/Computational Details

Molecular Dynamics (MD) simulations of α-CD, β-CD, and γ-CD in water were performed by using the GROMACS software (version 2023) [38]. Fig. 1 shows the numbering of oxygen atoms. In all cases, a cubic box with periodic boundary conditions contained a CD and 3500 water molecules. The equations of motion were integrated using the leapfrog algorithm with a time step of 1 fs. The long-range electrostatic force calculations used the particle-mesh Ewald algorithm. [39,40] A short, two ns equilibration under NPT conditions used the Berendsen thermostat and barostat [41] to generate velocities from a random Maxwell-Boltzmann distribution at 298 K. This was followed by a two ns equilibration under NVT conditions using the Berendsen thermostat at 298 K. Finally, a production run of 1250 ns was performed under NVT conditions at 298 K using the Nosé-Hoover thermostat [42,43]. Configurations were collected every 10000 ps for further analysis. For CD, the q4md-CD [19] force field was applied. Bond lengths were kept fixed by the LINCS algorithm.[44] The following water models were used to test their effect on the ratio of rotated state for the studied CDs: SPC [23], SPC/E [24], OPC3 [25], TIP3P [26], TIP4P/2005 [27], TIP5P [28]. Bond lengths and the bond angle of water molecules were constrained by applying the SHAKE algorithm.[45].

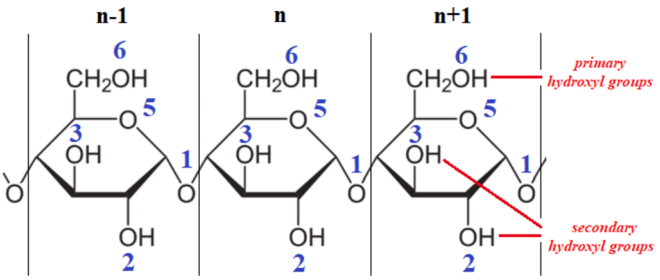

Fig. 1. Atom labels for two neighboring cyclodextrin units.

The box lengths were 4.75745 nm (SPC), 4.73602 nm (SPC/E), 4.74652 nm (OPC3), 4.74657 nm (TIP3P), 4.72711 nm (TIP4P/2005), 4.73645 nm (TIP5P) for α-CD; 4.76844 nm (SPC), 4.71854 nm (SPC/E), 4.73651 nm (OPC3), 4.74661 nm (TIP3P), 4.73433 nm (TIP4P/2005), 4.74896 nm (TIP5P) for β-CD; 4.75891 nm (SPC), 4.74129 nm (SPC/E), 4.73579 nm (OPC3), 4.75097 nm (TIP3P), 4.73918 nm (TIP4P/2005), 4.75859 nm (TIP5P) for γ-CD.

3. Results and discussion

3.1. Structural properties of CD molecules in the light of tumbling of Glcp units

The characteristic shape of CDs is determined by the conformation of their building block (α-D-Glc*p*) and the orientation of these sugar units relative to each other. The Glc*p* ring conformation types were determined by the puckering parameters, which were calculated by Ref. [46]. In line with the previous results [13], we found the α-D-Glc*p* units are in the $^4C_1$ type conformation in more than 95 % of cases for all three studied CDs. The relative orientation of a pair of consecutive Glc*p* units can be characterized by the dihedral angle ξ defined as $O2_nC1_nC4_{n-1}O3_{n-1}$. The CD molecule is classified in the rotated state when contains at least one rotated unit. One unit is considered rotated when ξ less than −70° or more than 70° according to Ref. [13]. The calculated ratio of rotated cases for six different water models applying q4md-CD forcefield for CD molecules can be found in Table 1. It should be noted that stricter condition also exists [19], namely $\xi < -60°$ or $\xi > 60°$, therefore values

Table 1
Percentages of time frames in which at least one glucopyranoside unit turned (%).

Systems	SPC	SPC/E	OPC3	TIP3P	TIP4P/2005	TIP5P
α-CD	5.72 (10.27)	6.94 (11.97)	12.55 (17.85)	6.98 (11.24)	9.26 (14.69)	58.66 (70.60)
β-CD	7.80 (18.15)	10.91 (21.52)	15.64 (26.42)	7.62 (18.42)	9.68 (20.44)	90.30 (95.23)
γ-CD	51.54 (62.71)	58.72 (67.38)	64.39 (72.85)	51.00 (62.05)	67.72 (75.384)	100.00 (100.00)

calculated in this way are reported in parentheses.

The ratios of the rotated frames were found to be the lowest for SPC and TIP3P water models, while the highest values arise in the case of TIP5P. For γ-CD, even the lowest value exceeds the 50 %. For α-CD and β-CD, the number of rotated frames is not as significant as for γ-CD. The lowest value is 5.72 % for the q4md-CD/SPC model of α-CD and 6.98 % for the q4md-CD/TIP3P model of β-CD. As a comparison, Gebhart et al. [13] reported that 6.17 %, 12.97 %, and 68.5 % of the time frames as rotated for α-, β-, and γ-CDs, respectively, during a 500 ns CHARMM36 simulation applying TIP3P water model. It is worth noting that the direct comparison impairs because these values are missing for their q4md-CD/TIP3P simulation.

The time series of the flip dihedral angle ξ from q4md-CD/TIP3P models according to our calculations can be seen in Fig. 2. It is necessary to point out that the TIP3P water model was chosen to compare the results with those of the previous study, where applicable. [7,13,19] In the case of α-CD (Fig. 2a), the sugar unit returns to its original state shortly after it is turned out, while the rotated case can persist for a longer time (up to 25 ns) for β-CD (Fig. 2b). For γ-CD (Fig. 2c), we observed that the rotated state can remain stable even longer than 300 ns. Our results are in line with the findings of earlier studies. [13,19].

Additionally, though not mentioned previously, in the case when one unit in α-CD turns outward, the deviation of ξ angle is generally larger than that of for β-CD where the ξ angle of the rotated unit stays near the angle limit between the rotated and non-rotated states. This behavior is shown in the flip dihedral angle distribution (Fig. 2d and e), where the function is narrower for α-CD than for β-CD. In α-CD, a smaller peak appears on either side of the main peak. Although the main peaks are separated by two distinct maxima, β-CD lacks these secondary peaks. In the case of γ-CD, the distribution (Fig. 2f) is more spread and shows more prominently both features (double and side peaks) than in the previous two cases.

Fig. 3a–c shows detailed statistics about the number of the rotated units. For even numbers of *Glcp units*, considering only the rotated cases, the most common case is when two *Glcp units* rotate. The probability of this case is 4.8 % for α-CD and 27 % for γ-CD. The insets show that 97 % and 65 % of these rotated units are adjacent in α-CD and γ-CD, respectively. In the case of β-CD with uneven Glc*p* unit, only one unit is rotated in most cases (6.2 %). The occurrence of two rotated units is minimal (0.89 %), but when it does occur, the two rotated units are mostly (66 %) adjacent.

Two glycosyl dihedral angles ϕ and ψ are defined as $O5_nC1_nO1_nC4_{n-1}$ and $C1_nO1_nC4_{n-1}C3_{n-1}$, respectively (cf. Fig. 1). The ϕ and ψ values in Table 2 depend on the state of the Glc*p* units, i.e., whether only one is in the regular or inverted state. For the α- and β-CD, where the ratio of rotated units is lower, the average value only slightly differs from the non-rotated ones. The ζ ($O2_nC2_nC3_nO3_n$) dihedral angle associated with two secondary OH orientations within the same Glc*p* unit did not show significant differences between the two configurations (rotated and not-rotated). These results are in good agreement with the data from Refs. [10,13,19].

Joint probability distributions are shown in Fig. 4 for the non-rotated state of all the studied CDs. Furthermore, the difference between the non-rotated and rotated cases is plotted with colors. Concerning P (ω($O5_nC5_nC6_nO6_n$)-υ($C5_nC6_nO6_nH6_n$)) distribution (Fig. 4a), the gt-tg combination has the highest occurrence, that is almost 50 % for α-CD and is close to 40 % for both the β-CD and for γ-CD. On the other hand, the population of the other two conformations with significant contributions, the gg-gt and the gg-gg, is the smallest for α-CD. The difference between the rotated and non-rotated state is the most significant for α-CD (marked by red in Fig. 4a), which exceeds the 30 % of the occurrences of the non-rotated case for gg-gg and gg-gt conformations, and the 20 % for gt-gg and gt-tg ones.

In Fig. 4b for P(θ($C2_nC3_nO3_nH3_n$)-φ ($C3_nC2_nO2_nH2_n$)), the most stable conformation is the gt-gg, and its value emerges for γ-CD. Furthermore, the gg-tg, the gt-tg, and the tg-gg conformers are significant. Concerning the mentioned four conformations, the highest difference between the non-rotated and rotated states can be observed in the case of tg-gg conformation for α-CD, which exceeds half of the population of the non-rotated state. Furthermore, the difference is important in the gt-gg conformation of β-CD and gg-tg for all studied CDs. It should be noted that no trend was found due to the increasing

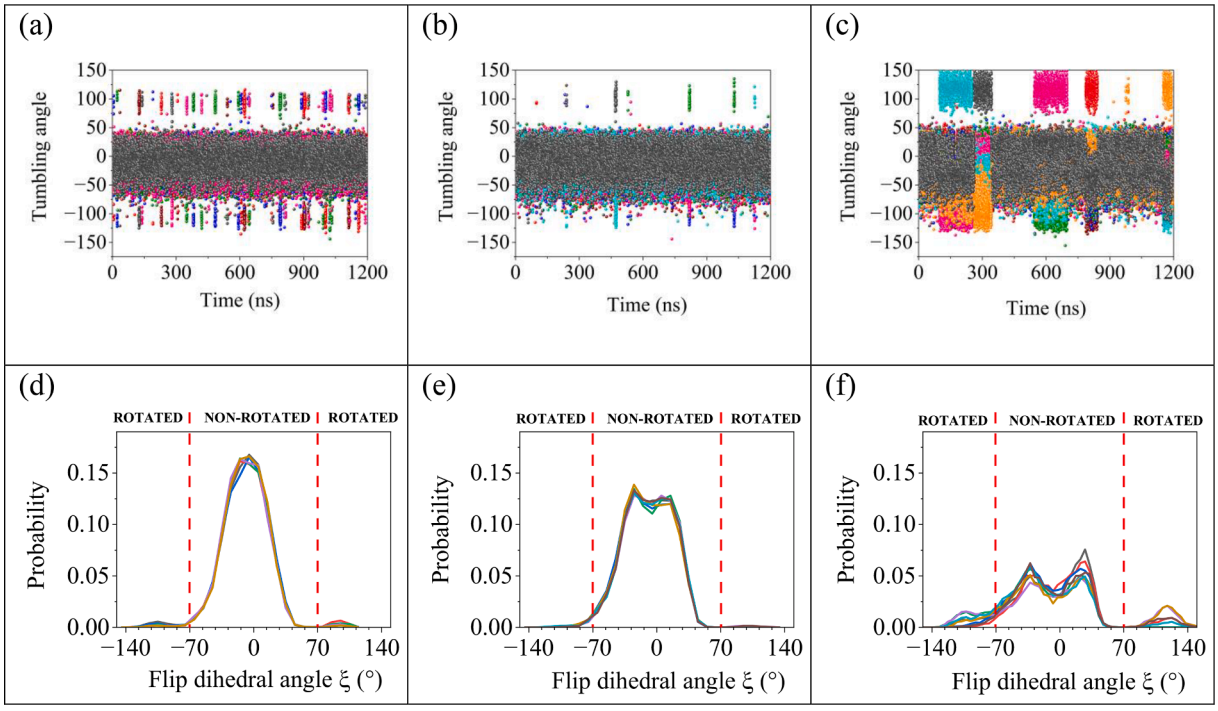

Fig. 2. Time series of the flip dihedral angle ξ for (a) α-CD, (b) β-CD and (c) γ-CD from the 1250 ns simulation. The different colors represent the different Glc*p* units. Distribution of the flip dihedral angle ξ (d) for α-CD, (e) for β-CD, and (f) for γ-CD.

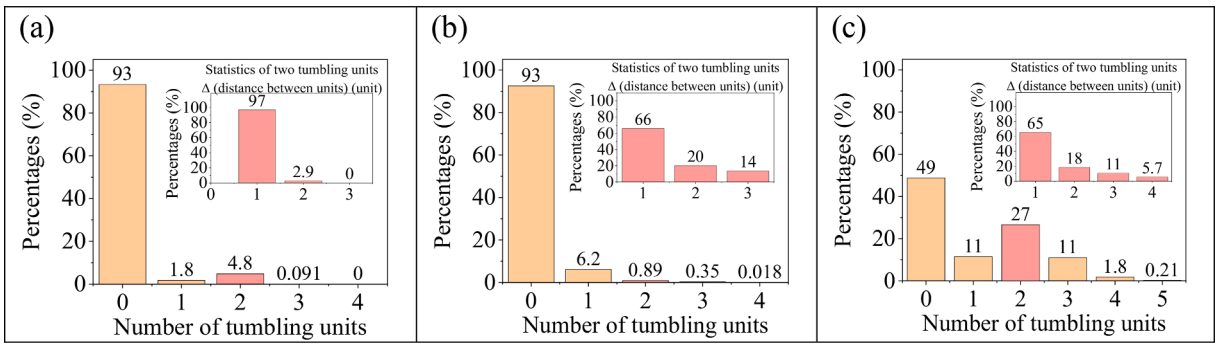

Fig. 3. Time evolution of tumbling for different Glc*p* units for (a) for α-CD, (b) for β-CD, and (c) for γ-CD. Number of tumbling units (d) for α-CD, (e) for β-CD, and (f) for γ-CD.

Table 2
Structural properties of the studied CDs obtained from MD simulations (q4md-CD/TIP3P model), compared with results from simulation and experiment. (Errors are in parentheses.)

	α-CD			β-CD			γ-CD		
	ϕ	ψ	ζ	ϕ	ψ	ζ	ϕ	ψ	ζ
Non-rotated	111.0 (±0.2)	122.1 (±2.7)	65.7 (±0.1)	113.9 (±0.7)	122.2 (±3.4)	68.0 (±0.1)	109.6 (±3.5)	108.2 (±5.0)	64.8 (±0.1)
Rotated	112.1 (±0.2)	124.8 (±2.7)	65.7 (±0.1)	114.2 (±0.7)	122.7 (±3.4)	68.0 (±0.1)	117.0 (±3.5)	122.9 (±5.0)	64.8 (±0.1)
Average	111.1 (±0.2)	122.3 (±2.7)	65.7 (±0.1)	113.9 (±0.7)	122.3 (±3.4)	68.0 (±0.1)	113.4 (±3.5)	115.7 (±5.0)	64.8 (±0.1)
Average from [19]	109.4	127.7	68.1	112.1	125.0	67.8	113.3	123.5	67.5
Average from [13]	111.7	126.3	69.6	111.9	125.0	69.4	105.1	128.4	69.0
Experiment [10]	109.2	128.8	–	109.8	127.6	–	108.9	127.1	–

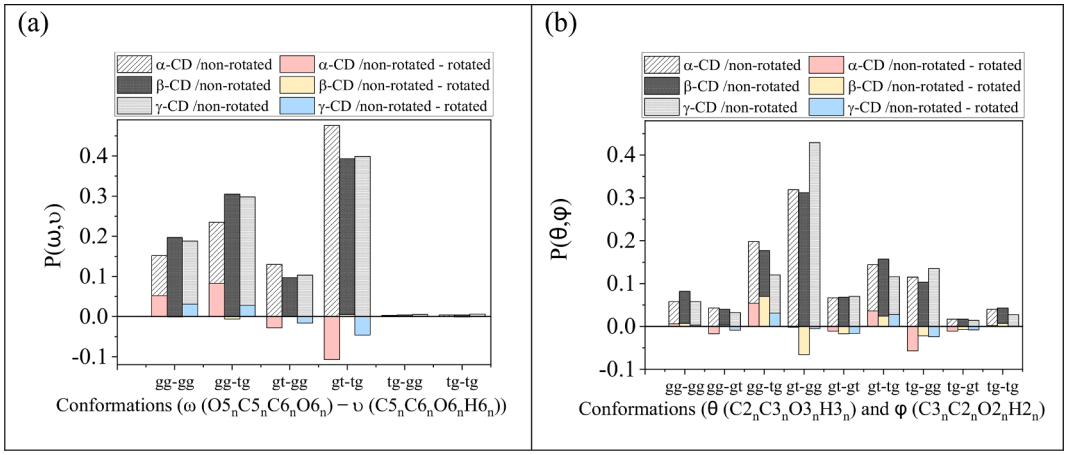

Fig. 4. Joint probability distribution defined by the dihedral angle (a) ω ($O5_nC5_nC6_nO6_n$) and υ ($C5_nC6_nO6_nH6_n$), (b) θ($C2_nC3_nO3_nH3_n$) and φ ($C3_nC2_nO2_nH2_n$). Conformations are classified as gg, gt, and tg when the characterizing dihedral angle is in the range (−120, 0), (0,120), and (120, −120), respectively.

number of Glc*p* units in the studied CDs. One exception is the population of gg-tg conformation decreases with the increasing size of the CD molecule.

3.2. Intramolecular H-bond network

In the CD molecule, three oxygen atoms can participate in intramolecular H-bond formation: two secondary hydroxyl oxygen atoms (O2 and O3), as well as the primary hydroxyl oxygen (O6) (see numbering in Fig. 1). Based on geometric criteria, we monitor possible H-bond formation applying the following two definitions: (1) the OH distance is less than 2.5 Å and the O…O-H angle is less than 30°, (2) the OH distance is less than 2.5 Å and the O…O-H angle is less than 60°. It is worth pointing out that a more permissive condition for the H-bond angle is required to reveal the connections between O2 and O3 oxygen atoms in the same Glc*p* unit. Table 3 contains the calculated distances and angles of the intramolecular (inter-unit and intra-unit) H-bonds between the primary and the secondary OH groups. Values were normalized with the probability of the H-bond occurrences. The inter-unit H-bond distances between the secondary OH groups ($O2_nH2_n$…$O3_{n-1}$, $O3_nH3_n$…$O2_{n+1}$) decrease as the number of Glc*p* units increases in the case of 30° angle criteria were applied to determine the H-bond. The magnitude of the decrease is 0.03–0.05 Å. This behavior is in good agreement with that observed for CD crystal hydrates. [10–12].

Concerning the H-bonds between the secondary OH groups (connecting to O2 and O3) the average H-bond distances between OH groups in the same Glc*p* unit are significantly longer than those between the neighboring units. The average angle of intra-unit H-bonds ($O2_n$-$H2_n$…

Table 3
Average distances and angles of intramolecular hydrogen bonds in CDs.

	α-CD		β-CD		γ-CD	
	Def.1.	Def.2.	Def.1.	Def.2.	Def.1.	Def.2.
(a) Calculated from the whole trajectory						
$O2_nH2_n…O3_{n-1}$ (Å)	1.993	2.017	1.971	1.994	1.941	1.963
$O3_nH3_n…O2_{n+1}$ (Å)	1.936	1.944	1.924	1.933	1.923	1.934
$O2_nH2_n…O3_n$ (Å)	0	2.306	0	2.369	0	2.299
$O3_nH3_n…O2_n$ (Å)	0	2.295	0	2.360	0	2.280
$O6_nH_n…O6_{n-1}$ (Å)	2.060	2.108	2.100	2.166	2.070	2.136
$O2_n$-$H2_n…O3_{n-1}$ (°)	14.455	16.228	14.448	16.189	13.382	14.974
$O3_n$-$H3_n…O2_{n+1}$ (°)	10.898	11.449	11.160	11.811	11.398	12.206
$O2_n$-$H2_n…O3_n$ (°)	0	51.653	0	52.346	0	51.746
$O3_n$-$H3_n…O2_n$ (°)	0	51.104	0	51.897	0	50.884
$O6_n$-H_n-$O6_{n-1}$ (d°)	17.499	21.617	18.749	24.795	17.656	23.364
(b) Calculated from the frames without rotated unit						
$O2_nH2_n…O3_{n-1}$ (Å)	1.994	2.017	1.963	1.986	1.936	1.958
$O3_nH3_n…O2_{n+1}$ (Å)	1.937	1.944	1.928	1.938	1.925	1.936
$O2_nH2_n…O3_n$ (Å)	0	2.307	0	2.362	0	2.290
$O3_nH3_n…O2_n$ (Å)	0	2.297	0	2.352	0	2.270
$O6_nH_n…O6_{n-1}$ (Å)	2.063	2.110	2.105	2.173	2.069	2.135
$O2_n$-$H2_n…O3_{n-1}$ (°)	14.480	16.247	13.956	15.602	13.062	14.587
$O3_n$-$H3_n…O2_{n+1}$ (°)	10.890	11.441	11.217	11.922	11.371	12.159
$O2_n$-$H2_n…O3_n$ (°)	0	51.660	0	52.214	0	51.557
$O3_n$-$H3_n…O2_n$ (°)	0	51.137	0	51.762	0	50.660
$O6_n$-H_n-$O6_{n-1}$ (°)	17.464	21.574	18.657	24.878	17.573	23.235
(c) Calculated from the frames with rotated unit						
$O2_nH2_n…O3_{n-1}$ (Å)	1.976	2.003	1.972	1.996	1.943	1.965
$O3_nH3_n…O2_{n+1}$ (Å)	1.922	1.930	1.924	1.932	1.923	1.934
$O2_nH2_n…O3_n$ (Å)	0	2.293	0	2.371	0	2.302
$O3_nH3_n…O2_n$ (Å)	0	2.275	0	2.362	0	2.284
$O6_nH_n…O6_{n-1}$ (Å)	2.038	2.088	2.099	2.165	2.070	2.136
$O2_n$-$H2_n…O3_{n-1}$ (°)	13.860	15.761	14.537	16.294	13.5	15.117
$O3_n$-$H3_n…O2_{n+1}$ (°)	11.098	11.657	11.149	11.791	11.408	12.223
$O2_n$-$H2_n…O3_n$ (°)	0	51.556	0	52.373	0	51.817
$O3_n$-$H3_n…O2_n$ (°)	0	50.721	0	51.924	0	50.973
$O6_n$-H_n-$O6_{n-1}$ (°)	17.833	22.032	18.763	24.782	17.685	23.409

$O3_n$, $O3_n$-$H3_n…O2_n$) is around 50° for all studied CDs. Therefore using the stricter H-bond definition for angles, namely the 30°, these intra-unit connections are not detectable.

It is interesting to note, that the orientation of the inter-unit hydrogen bonds both in the narrower rim and the wider rim can be clockwise or counterclockwise [8,9]. Our results show that there may be a smaller difference between the two cases, but this is not the subject of our article, more detail can be found in [8,9].

Fig. 5 shows the occurring probabilities of the H-bonds between each OH group within the CD molecule for α-CD, β-CD, and γ-CD. We used definition 2 of H-bond and applied for the whole trajectory without separated rotated and non-rotated configurations because, for these two systems, the low ratio of rotated cases did not cause differences in the results. We can identify both three type H-bond connections ($O2_nH2_n…O3_{n-1}$, $O2_nH2_n…O3_n$, $O6_nH_n$-$O6_{n-1}$), but their probabilities of occurrence are different (c.f. Fig. 5c). The highest probabilities belong to H-bonds between secondary OH groups of neighboring Glc*p* units ($O2_nH2_n…O3_{n-1}$). On the other hand, H-bonds are somewhat less likely to appear between secondary hydroxyl groups in the same unit ($O2_nH2_n…O3_n$). Compared to these two cases, the probability of developing an H-bond between the consecutive primary OH groups ($O6_nH_n$-$O6_{n-1}$) is significantly lower. It is necessary to point out, that we also found connections between non-neighbouring primary OH groups, but with extremely low probabilities. Comparing these values to the three CD systems, the value for α-CD is somewhat higher.

The differences in the occurring probabilities of H-bond between rotated and non-rotated configurations are plotted in Fig. 6 for γ-CD. Differences can be detected only relating to H-bonds between secondary hydroxyls. H-bonding shows different behavior in the clockwise and the counterclockwise directions. The H-bond probabilities are significantly

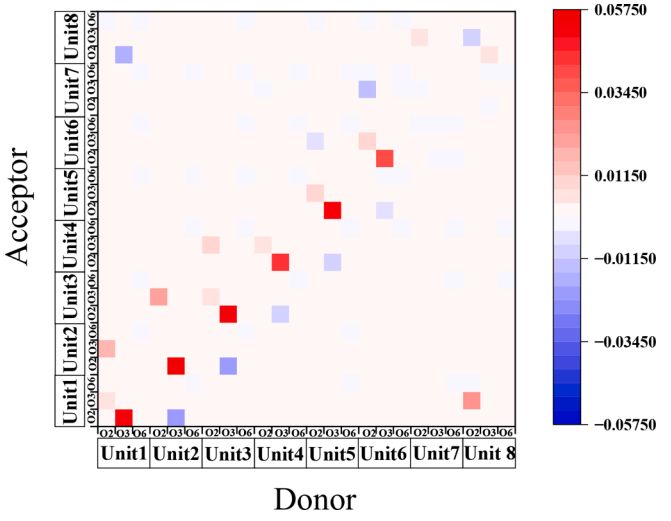

Fig. 6. Two-dimensional representation of the differences of the occurring probabilities of H-bond between rotated and non-rotated configurations for γ-CD.

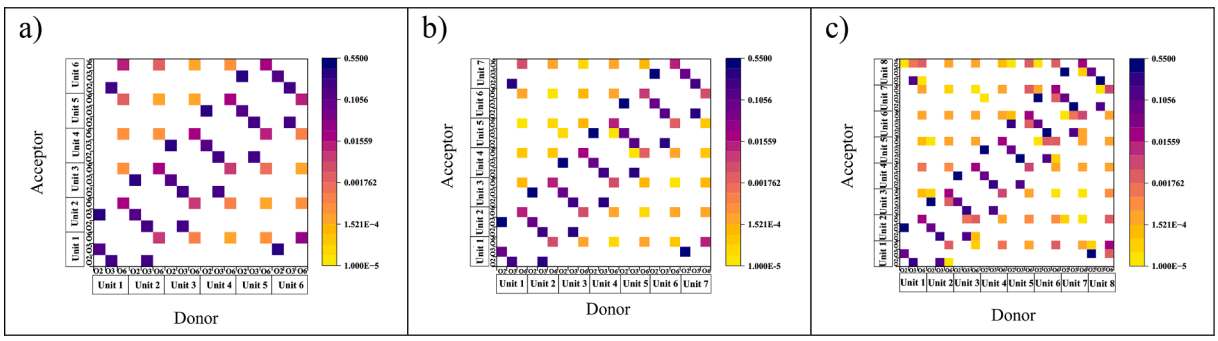

Fig. 5. Two-dimensional representation of the H-bond occurring probabilities (a) for α-CD, (b) for β-CD, and (c) for γ-CD.

higher in the rotated case between intra-unit secondary hydroxyl groups.

Table 4 contains the calculated average fraction of H-bonds for the whole trajectory using the above-defined two different H-bond definitions. It can be stated that the highest probability of forming an H-bond is with adjacent secondary OH. This is not affected by whether there is a rotated Glc*p* unit in the molecule. The highest value was obtained for β-CD. Note that there was no distinction made between clockwise and counterclockwise directions for the H-bonds in the case of those hydroxyl groups connected to O2 and O3. The number of H-bonds formed is symmetrical in terms of acceptor–donor ratios. Half of the bonds are donor and half are acceptor types. [7].

The size distribution of the clusters formed by H-bonds between secondary OH groups is shown in Fig. 7. It is important to remember that both intra-unit ($O2H2_n…O3_n$) and inter-unit ($O2H2_n…O3_{n-1}$) connections are considered. Thus, the maximum number of H-bonded members, i.e. the size of the cluster, which runs around the wider rim, is 12. 14. and 16 for α-CD. β-CD and γ-CD, respectively. We found that the probability of forming a full H-bonded ring exceeds 0.01. This is the highest value for all three systems from those cases, where the ring consists of more than one member. This represents a significantly larger value than the value calculated directly from the inter-unit and intra-unit H-bonding probability. This suggests that a significant cooperative effect was detected. Fig. 7b shows for α-CD that this percolated H-bonded chain is also observed in that configuration when at least one Glc*p* unit turns upside down.

3.3. Small-angle X-ray scattering experiments

Fig. 8 shows the small-angle X-ray scattering (SAXS) signals for two concentrations (c.f. Material Section) of the three studied CDs. A significant characteristic feature of the diffraction experiment (Fig. 8a) is the existence of intensity maxima, which in our case were found around 8.5 nm^{-1}, 7.1 nm^{-1}, and 6.3 nm^{-1} for α-, β-, and γ-CD respectively. These values are almost the same in the case of both concentrations. The position of the peak maxima shifts to higher values as the number of sugar units decreases. Such features were also detected in the aqueous solution of CD molecules [32,33].

In Fig. 8b the lower Q region, namely the Guinier region ($Q_{max}{\cdot}R_g < 1.0$) is well visible in all solutions. This range (0–1.0 nm^{-2}) of ln(I) vs. q^2 shows a linear behaviour. With the help of fitting procedure we determined the Guinier radius (R_g) for α-, β-,and γ-CD molecules. The values, given in Table 5, agree well with the results obtained by Kusmin et al. [31] from SAXS and SANS studies of dilute solutions. We calculated the Guinier radius [29] from the simulation, which shows reasonable agreement with experimental data.

There is considerable debate in the literature about whether CD molecules aggregate in aqueous solution. [47] Photon correlation experiments, osmotic coefficient data, and light scattering experiments [48,49] suggest aggregations in aqueous solutions of the order of 100 nm. On the other hand, the existence of such aggregations is highly questionable based on NMR experimental data [47] and previous small-angle diffraction experiments [31]. The only sign in our experiment that may indicate aggregation is the slight increase in the intensity in the small Q region of the γ-CD. However, we have to point out that these aggregations occur in very small proportions and only in γ-CD.

We calculated from MD simulations the scattered intensity of the molecule (molecular form factor) for the structure of the non-rotated and the rotated types of CD molecules, according to the Debye formalism, using the equation.

$$I(q) = \sum_{i=1}^{N}\sum_{j=1}^{N}\frac{\sin(qr_{ij})}{qr_{ij}}f_i(q)f_j(q) \quad (1)$$

where q is the scattering vector, f_i and f_j are the atomic scattering factors of i and j sites, and r_{ij} is the distance between the i and j sites of CD. The resulting scattering curves are shown in Fig. 9. The intensity maxima determined from these curves are also can be found in the figure.

For all three studied CD systems, the maximum seen earlier in the experimental curves is also visible in the non-rotated case. These values agree well with the data determined from the experiment. However, no measurable intensity maximum was detected for systems containing rotated CD molecules. Based on these results, it can be concluded that the number of CD molecules turned out is very small even in the case of γ-CD. (Note, that in the MD simulations of γ-CD, the rotated case exceeds 50 %.).

4. Conclusion

Molecular Dynamics simulations were complemented by small-angle X-ray scattering (SAXS) experiments to reveal (1) the phenomenon of tumbling of Glc*p* unit [13,19] and (2) the intramolecular hydrogen bonding connections, as well as (3) the effects of tumbling on H-bond properties of CD molecule. MD simulations were performed on aqueous solutions of α-CD, β-CD, and γ-CD using q4md-CD forcefield for CD molecules [19]. Five different models were applied for water molecules to monitor the evolution of the ratio of rotated Glc*p* units over time during 1200 ns-long simulations.

The following results are worth highlighting concerning the tumbling of the Glc*p* unit:

(1) A comparison of molecular dynamics (MD) and small-angle X-ray scattering (SAXS) shows that the results of α-CD and β-CD simulations, where at least one Glcp unit rotates in 5–8 % of the time frames, better reflect the actual behavior of γ-CD. The SAXS experiment did not support the high prevalence of Glcp units (more than 50 % of the time frames) in the γ-CD in the rotated position.
(2) From the applied water models, the occurrence of the rotated glycopyranose unit was the lowest in the SPC and TIP3P water models. No significant differences were identified between these models.
(3) It was found that for α-CD and γ-CD when one unit turned in one direction, another unit typically rotated in the opposite direction at the same time. Furthermore, it is noticeable that these rotated units are mainly each other's neighbors. This observation, however, does not apply to β-CD.

Regarding the intramolecular H-bond properties, we were able to make the following observations:

(1) To reveal the interactions of the secondary hydroxyl groups within the same Glc*p* unit, it was necessary to define a more permissive H-bonding definition in terms of angle.
(2) H-bonds calculated from simulations suggest the formation of cooperative H-bonded rings between secondary adjacent hydroxyl groups of neighboring Glc*p* units.

Table 4
The average fraction of H-bonds is calculated for the whole trajectory using the above-defined two different H-bond definitions.

		Non-rotated		Rotated	
		Def.1.	Def.2.	Def.1.	Def.2.
α-CD	$O2H2_n…O3_n/O3H3_n…O2_n$	0	0.46	0	0.49
	$O2H2_n…O3_{n-1}/O3H3_n…O2_{n-1}$	0.71	0.75	0.40	0.42
	$O6H_n…O6_{n-1}$	0.03	0.04	0.05	0.06
β-CD	$O2H2_n…O3_n/O3H3_n…O2_n$	0	0.31	0	0.31
	$O2H2_n…O3_{n-1}/O3H3_n…O2_{n-1}$	0.80	0.85	0.63	0.67
	$O6H_n…O6_{n-1}$	0.01	0.02	0.02	0.03
γ-CD	$O2H2_n…O3_n/O3H3_n…O2_n$	0.01	0.50	0.02	0.51
	$O2H2_n…O3_{n-1}/O3H3_n…O2_{n-1}$	0.78	0.82	0.52	0.55
	$O6H_n…O6_{n-1}$	0.01	0.02	0.02	0.03

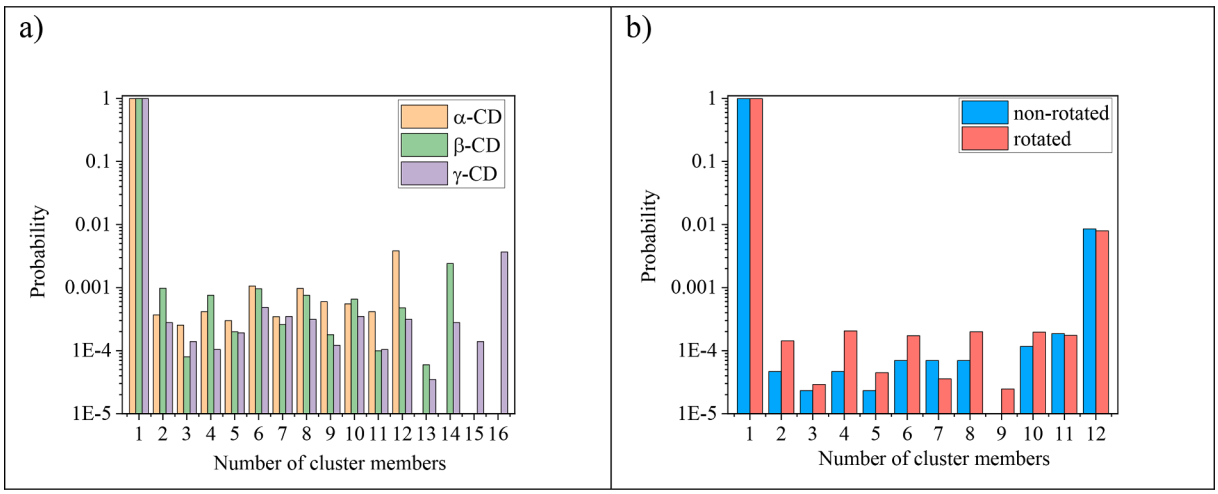

Fig. 7. Size distribution of H-bond clusters between secondary OH groups calculated a) for the three studied systems. b) for the rotated and the non-rotated cases of α-CD.

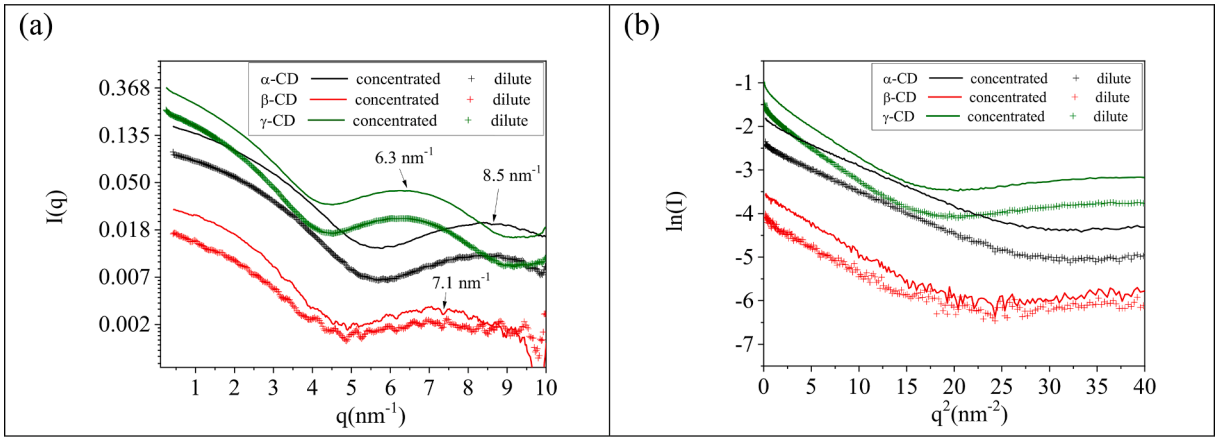

Fig. 8. (a) I(q) – q plot of the scattering intensity for the more concentrated solutions. (b) ln(I) – q^2 plot of the scattering intensity for two concentrations.

Table 5
Guinier radius (nm) for α-, β-, and γ-CD molecules from the experiments and simulation.

	experimental/diluted	experimental/concentrated	simulation
α-CD	0.630	0.590	0.560
β-CD	0.694	0.674	0.630
γ-CD	0.766	0.766	0.701

(3) It is essential to calculate the properties, that characterize H-bonds, separately for the rotated and non-rotated cases of γ-CD, especially since the ratios of the frames, where at least one Glc*p* unit rotated, were quite high (above 50 %) in the simulations.

Our goal in a future publication is to examine the impact of tumbling rates on the hydrogen bonding properties of the hydration shell of the CD molecule. Additionally, we aim to understand how these changes affect the overall structural properties of water molecules bonded to CD molecules through hydrogen bonds and those to hydrophobic surfaces.

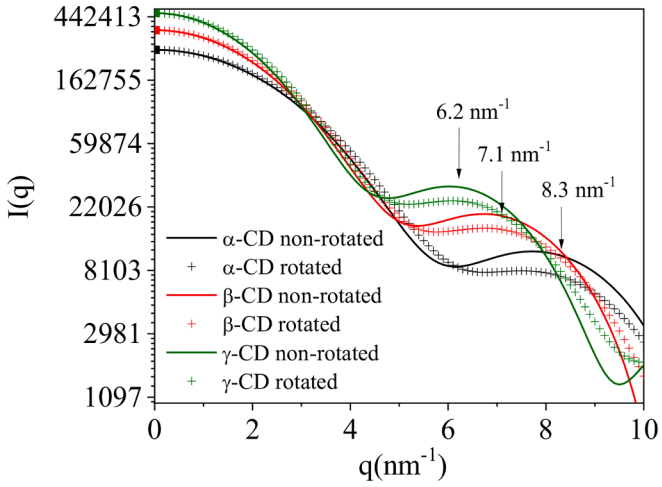

Fig. 9. Calculated molecular form factors for the three studied CDs in the case of rotated and non-rotated cases.

CRediT authorship contribution statement

Imre Bakó: Writing – review & editing, Writing – original draft, Software, Methodology, Investigation, Formal analysis, Data curation, Conceptualization. **András Wacha:** Writing – review & editing, Validation, Investigation, Data curation. **Szilvia Pothoczki:** Writing – review & editing, Writing – original draft, Visualization, Validation, Supervision, Investigation, Conceptualization.

Declaration of competing interest

The authors declare that they have no known competing financial interests or personal relationships that could have appeared to influence the work reported in this paper.

Acknowledgment

The authors are grateful to the National Research, Development and Innovation Office (NRDIO (NKFIH). Hungary) for financial support via grants Nos. 142429 (IB, SP), 146081 (AW), 2020-1.1.2-PIACI-KFI_2020 00021 and TKP2021-EGA-13. András Wacha acknowledges the support of the János Bolyai Research Fellowship of the Hungarian Academy of Sciences. The authors greatly appreciate helpful discussions with Dr. László Jicsinszky (University of Turin).

Data availability

Data will be made available on request.

References

[1] C. Sun, Z. Wei, C. Xue, L. Yang, Development, application and future trends of starch-based delivery systems for nutraceuticals: A review, Carbohydr. Polym. 308 (2023) 120675, https://doi.org/10.1016/j.carbpol.2023.120675.
[2] J. Szejtli, Introduction and General Overview of Cyclodextrin Chemistry, Chem. Rev. 98 (5) (1998) 1743–1754, https://doi.org/10.1021/cr970022c.
[3] M.E. Davis, M.E. Brewster, Cyclodextrin-based pharmaceutics: Past, present and future, Nat. Rev. Drug Discov. 3 (2004) 1023–1035, https://doi.org/10.1038/nrd1576.
[4] B. Tian, J. Liu, Cyclodextrin-metal-organic frameworks in molecular delivery, detection, separation, and capture: An updated critical review, Carbohydrate Polymer 306 (2023) 120598, https://doi.org/10.1016/j.carbpol.2023.120598.
[5] V. Aiassa, C. Garnero, M.R. Longhi, A. Zoppi, Cyclodextrin Multicomponent Complexes: Pharmaceutical Applications, Pharmaceutics 13 (7) (2021) 1099, https://doi.org/10.3390/pharmaceutics13071099.
[6] G. Fang, X. Yang, S. Chen, Q. Wang, A. Zhang, B. Tang, Cyclodextrin-based host-guest supramolecular hydrogels for local drug delivery, Coord. Chem. Rev. 454 (2022) 214352, https://doi.org/10.1016/j.ccr.2021.214352.
[7] A.A. Sandilya, U. Natarajan, M.H. Priya, Molecular View into the Cyclodextrin Cavity: Structure and Hydration, ACS Omega 5 (40) (2020) 25655–25667, https://doi.org/10.1021/acsomega.0c02760.
[8] A. Stachowicz, A. Styrcz, J. Korchowiec, A. Modaressi, M. Rogalski, DFT studies of cation binding by β-cyclodextrin, Theor. Chem. Acc. 130 (2011) 939–953, https://doi.org/10.1007/s00214-011-1014-9.
[9] W. Snor, E. Liedl, P. Weiss-Greiler, A. Karpfen, H. Viernstein, P. Wolschann, On the structure of anhydrous β-cyclodextrin, Chem. Phys. Lett. 441 (2007) 159–162, https://doi.org/10.1016/j.cplett.2007.05.007.
[10] W. Saenger, J.L. Jacob, K. Gessler, T. Steiner, D. Hoffmann, H. Sanbe, K. Koizumi, S.M. Smith, T. Takaha, Structures of the Common Cyclodextrins and Their Larger Analoguess – Beyond the Doughnut, Chem. Rev. 98 (1998) 1787–1802, https://doi.org/10.1021/cr9700181.
[11] W. Saenger, M. Noltemeyer, P. Manor, B. Hingerty, B. Klar, Induced-Fit"-Type Complex Formation of the Model Enzyme α-Cyclodextrin, Bioorg. Chem. 5 (1976) 187–195, https://doi.org/10.1016/0045-2068(76)90007-9.
[12] W. Saenger, C. Betzel, B. Hingerty, G.M. Brown, Flip-Flop Hydrogen Bonds in β-Cyclodextrin - A Generally Valid Principle in Polysaccharides, Angew. Chem. Int. Ed. Engl. 22 (1983) 883–884, https://doi.org/10.1002/anie.198308831.
[13] J. Gebhardt, C. Kleist, S. Jakobtorweihen, N. Hansen, Validation and Comparison of Force Fields for Native Cyclodextrins in Aqueous Solution, J. Phys. Chem. B 122 (2018) 1608–1626, https://doi.org/10.1021/acs.jpcb.7b11808.
[14] Y. Liu, C. Chipot, X. Shao, W. Cai, Threading or Tumbling? Insight into the Self-Inclusion Mechanism of an altro-α-Cyclodextrin Derivative, J. Phys. Chem. C 118 (2014) 19380–19386, https://doi.org/10.1021/jp503866q.
[15] J. Terao, Y. Konoshima, A. Matono, H. Masai, T. Fukjihara, Y. Tsuji, Synthesis of an Organic-Soluable π-Conjugated [3]Rotaxane Via Rotation of Glucopyranose Units in Permethylated β-Cyclodextrin, Beilstein J. Org. Chem. 10 (2014) 2800–2808, https://doi.org/10.3762/bjoc.10.297.
[16] K. Yamauchi, A. Miyawaki, Y. Takashima, H. Yamaguchi, A. Harada, Switching from Altro-α-Cyclodextrin Dimer to Pseudo[1]-Rotaxane Dimer through Tumbling, Org. Lett. 12 (2010) 1284–1286, https://doi.org/10.1021/ol1001736.
[17] Y. Takashima, Y. Fukui, M. Otsubo, N. Hamada, H. Yamaguchi, H. Yamamoto, A. Harada, Emission Properties of Cyclodextrin Dimers Linked with Perylene Diimide - Effect of Cyclodextrin Tumbling, Polym. J. 44 (2012) 278–285, https://doi.org/10.1038/pj.2011.128.
[18] V. Legros, C. Vanhaverbeke, F. Souard, C. Len, J. Désiré, β-Cyclodextrin–Glycerol Dimers: Synthesis and NMR Conformational Analysis, J. Org. Chem. 13 (2013) 2583–2590, https://doi.org/10.1002/ejoc.201201716.
[19] C. Cezard, X. Trivelli, F. Aubry, F. Djedaïni-Pilard, F. Dupradeau, Molecular Dynamics Studies of Native and Substituted Cyclodextrins in Different Media: 1. Charge Derivation and Force Field Performances, Phys. Chem. Chem. Phys. 13 (2011) 15103–15121, https://doi.org/10.1039/C1CP20854C.
[20] I. Bakó, L. Jicsinszky, S. Pothoczki, Systematic Study of Different Types of Interactions in α-, β- and γ-Cyclodextrin: Quantum Chemical Investigation, Molecules 29 (10) (2024) 2205, https://doi.org/10.3390/molecules29102205.
[21] S. Pereva, V. Nikolova, S. Angelova, T. Spassov, T. Dudev, Water inside β-cyclodextrin cavity: amount, stability and mechanism of binding Beilstein, J. Org. Chem. 15 (2019) 1592–1600, https://doi.org/10.3762/bjoc.15.163.
[22] G. Wenz, Influence of intramolecular hydrogen bonds on the binding potential of methylated β-cyclodextrin derivatives, Beilstein J. Org. Chem. 8 (2012) 1890–1895, https://doi.org/10.3762/bjoc.8.218.
[23] H.J.C. Berendsen, J.P.M. Postma, W.F. van Gunsteren, J. Hermans, Interaction models for water in relation to protein hydration, in: B. Pullman (Ed.), Intermolecular Forces, D. Reidel Publishing Company, Dordrecht, 1981, pp. 331–342.
[24] H.J.C. Berendsen, J.R. Grigera, T.P. Straatsma, The missing term in effective pair potentials, J. Phys. Chem. 91 (1987) 6269–6271, https://doi.org/10.1021/j100308a038.
[25] S. Izadi, A.V. Onufriev, Accuracy limit of rigid 3-point water models, J. Chem. Phys. 145 (2016) 074501, https://doi.org/10.1063/1.4960175.
[26] W.L. Jorgensen, J. Chandrasekhar, J.D. Madura, R.W. Impey, M.L. Klein, Comparison of simple potential functions for simulating liquid water, J. Chem. Phys. 79 (1983) 926–935, https://doi.org/10.1063/1.445869.
[27] J.L.F. Abascal, C. Vega, A general purpose model for the condensed phases of water: TIP4P/2005, J. Chem. Phys. 123 (2005) 234505, https://doi.org/10.1063/1.2121687.
[28] M.W. Mahoney, W.L. Jorgensen, A five-site model for liquid water and the reproduction of the density anomaly by rigid, nonpolarizable potential functions, J. Chem. Phys. 112 (2000) 8910–8922, https://doi.org/10.1063/1.481505.
[29] A. Guinier, G. Fournet, Small-Angle Scattering of X-Rays, John Wiley & Sons, New York, 1955.
[30] H. Nirschl, X. Guo, Characterisation of structured and functionalized particles by small-angle X-ray scattering (SAXS), Chem. Eng. Res. Des. 136 (2018) 431–446, https://doi.org/10.1016/j.cherd.2018.06.012.
[31] A. Kusmin, R.E. Lechner, M. Kammel, W. Saenger, Native and Methylated Cyclodextrins with Positive and Negative Solubility Coefficients in Water Studied by SAXS and SANS, J. Phys. Chem. B 112 (112) (2008) 12888–12898, https://doi.org/10.1021/jp802031w.
[32] A. Triolo, F. Lo Celso, O. Russina, Structural Features of β-Cyclodextrin Solvation in the Deep Eutectic Solvent, Reline, J. Phys. Chem. B 124 (2020) 2652–2660, https://doi.org/10.1021/acs.jpcb.0c00876.
[33] A. Triolo, F. Lo Celso, J. Perez, O. Russina, Solubility and solvation features of native cyclodextrins in 1-ethyl-3-methylimidazolium acetate, Carbohydrate Polymers 291 119622 (2022), https://doi.org/10.1016/j.carbpol.2022.119622.
[34] D. Lombardo, A. Longo, R. Darcy, A. Mazzaglia, Structural Properties of Nonionic Cyclodextrin Colloids in Water, Langmuir 20 (2004) 1057–1064, https://doi.org/10.1021/la035370q.
[35] K.-C. Shih, C.-Y. Li, W.-H. Li, H.-M. Lai, Fine structures of self-assembled beta-cyclodextrin/Pluronic in dilute and dense systems: a small angle X-ray scattering study, Soft Matter 10 (2014) 7606–7614, https://doi.org/10.1039/C4SM01147C.
[36] A. Wacha, Z. Varga, A. Bóta, CREDO: a new general-purpose laboratory instrument for small-angle X-ray scattering, J. Appl. Cryst. 47 (2014) 1749–1754, https://doi.org/10.1107/S1600576714019918.
[37] A. Wacha, Optimized pinhole geometry for small-angle scattering, J. Appl. Cryst. 48 (2015) 1843–1848, https://doi.org/10.1107/S1600576715018932.
[38] D. van der Spoel, E. Lindahl, B. Hess, G. Groenhof, A.E. Mark, H.J. Berendsen, GROMACS: fast, flexible, and free, J. Comp. Chem. 26 (2005) 1701–1718, https://doi.org/10.1002/jcc.20291.
[39] T. Darden, D. York, L. Pedersen, Particle mesh Ewald: An N·log(N) method for Ewald sums in large systems, J. Chem. Phys. 98 (1993) 10089–10092, https://doi.org/10.1063/1.464397.
[40] U. Essman, L. Perera, M.L. Berkowitz, T. Darden, H. Lee, L.G. Pedersen, A smooth particle mesh Ewald method, J. Chem. Phys. 103 (1995) 8577–8593, https://doi.org/10.1063/1.470117.
[41] H.J.C. Berendsen, J.P.M. Postma, W.F. van Gunsteren, A. DiNola, J.R. Haak, Molecular Dynamics with Coupling to an External Bath, J. Chem. Phys. 81 (1984) 3684–3690, https://doi.org/10.1063/1.448118.
[42] S. Nosé, A molecular dynamics method for simulations in the canonical ensemble, Mol. Phys. 52 (1984) 255–268, https://doi.org/10.1080/00268978400101201.
[43] W.G. Hoover, Canonical dynamics: Equilibrium phase-space distributions, PhysRevA 31 (1985) 1695–1697, https://doi.org/10.1103/PhysRevA.31.1695.
[44] B. Hess, H. Bekker, H.J.C. Berendsen, J.G.E.M. Fraaije, LINCS: A linear constraint solver for molecular simulations, J. Comp. Chem. 18 (1997) 1463–1472, https://doi.org/10.1002/(SICI)1096-987X(199709)18:12<1463::AID-JCC4>3.0.CO;2-H.
[45] S. Miyamoto, P.A. Kollman, Settle: An analytical version of the SHAKE and RATTLE algorithm for rigid water models, J. Comput. Chem. 13 (1992) 952–962, https://doi.org/10.1002/jcc.540130805.
[46] D. Cremer, J.A. Pople, General definition of ring puckering coordinates, J. Am. Chem. Soc. 97 (1975) 1354–1358, https://doi.org/10.1021/ja00839a011.

[47] A.J.M. Valente, R.A. Carvalho, O. Söderman, Do Cyclodextrins Aggregate in Water? Insight from NMR Experiments, Langmuir 31 (23) (2015) 6314–6320, https://doi.org/10.1021/acs.langmuir.5b01493.
[48] L. Szente, J. Szejtli, G.L. Kis, Spontaneous Opalescence of Aqueous Gamma-Cyclodextrin Solutions: Complex Formation or Self-Agregation? J. Pharm. Sci. 87 (6) (1998) 778–781, https://doi.org/10.1021/js9704341.
[49] G. González-Gaitano, P. Rodríguez, J.R. Isasi, M. Fuentes, G. Tardajos, M. Sánchez, The Aggregation of Cyclodextrins as Studied by Photon Correlation Spectroscopy, J. Incl. Phenom. 44 (2002) 101–105, https://doi.org/10.1023/A:1023065823358.